LAWRENCE
LIVERMORE
NATIONAL
LABORATORY

LLNL-JRNL-410497

Strongly Driven Crystallization Processes in a Metallic Glass

T. LaGrange, D. S. Grummon, B. W. Reed, N. D. Browning, W. E. King, G. H. Campbell

February 11, 2009

Applied Physics Letters

Disclaimer

Thomas LaGrange, David S. Grummon, Bryan W. Reed, Nigel D. Browning, Wayne E. King, and Geoffrey. H. Campbell

Strongly Driven Crystallization Processes in a Metallic Glass

Applied Physics Letters

lagrange2@llnl.gov

Strongly Driven Crystallization Processes in a Metallic Glass

Thomas LaGrange[1], David S. Grummon[2], Bryan W. Reed[1], Nigel D. Browning[1,3], Wayne E. King[1], and Geoffrey H. Campbell[1]

[1]Lawrence Livermore National Laboratory, Physical and Life Sciences Directorate,7000 East Avenue, Livermore, California 94550, [2]Department of Chemical Engineering and Materials Science,2527 Engineering Blg,. Michigan State University, E. Lansing, Michigan 48824, [3]Department of Chemical Engineering and Materials Science, University of California, One Shields Avenue, Davis, California 95616

ABSTRACT

The crystallization of amorphous NiTi thin films was studied *in situ* using pulsed laser heating in a dynamic transmission electron microscope (DTEM). A single pulse can crystallize small areas of the film within 2 μs. The volume fraction of crystallized material and its morphology depend strongly on the laser energy, the spatial profile of the laser spot, and heat transport in the film. The microstructure developed under pulsed laser irradiation differs strongly from that which results from slower furnace and CW laser annealing protocols. High crystallization rates have been observed under pulsed irradiation that are not predicted by extrapolation of kinetic data obtained from slow-heating and isothermal crystallization experiments.

[Insert Physics and Astronomy Classificaiton Scheme Codes] Keywords: electron microscopy, metallic glasses, crystallization and Nitinol

Polymorphic crystallization processes have been extensively studied due to their industrial importance in materials engineering. Since nucleation and growth behavior determines crystal morphology and grain size, and thus influences resulting physical properties, most studies aim to accurately quantify nucleation and growth rates by thermal analysis, using techniques such as differential scanning calorimetry (DSC), and *in situ* heating in transmission electron microscopy (TEM). The desire to continually shrink thin film based devices and electronics, new material processing techniques have been developed using laser-based annealing to spatially control microstructure evolution on the micron and sub-micron scales. Nanosecond pulse laser annealing is particularly attractive since it limits the amount of peripheral heating and prevents unwanted microstructural changes to surrounding material. However, crystallization under pulsed laser irradiation can differ significantly from conventional thermal annealing, e.g., slow heating in a furnace. This means that quantifying the nucleation and growth rates by conventional thermal analysis do not reflect the mechanisms occurring under pulsed laser annealing, and as such, the connection with kinetic data to control processing parameters and tailor microstructures for desired technical applications breaks-down. As this paper will illustrate, this is especially true for amorphous NiTi materials, which have been used in shape memory thin film based microelectromechanical systems (MEMS)[1].

Here we show, by way of dynamic transmission electron microscope (DTEM) observations that the nucleation and growth behavior during crystallization of amorphous NiTi, when heated by pulsed laser induced crystallization, does indeed differ from that measured using DSC or conventional TEM. This discrepancy has also been observed in the amorphous to crystallization transition in other materials such as Si. For example,

Her et al. have compared crystallization kinetics of amorphous Si measured both under slow thermal annealing, and by pulsed laser irradiation, and have estimated activation energies for crystallization that are an order of magnitude lower under pulsed irradiation (0.18eV) than in DSC measurements (2.0 eV)[2]. Conversely, under continuous wave (CW) infrared laser annealing of NiTi films, nucleation and growth behavior are similar to conventional furnace annealed films, having activation energies of 5.72 and 3.03 eV, respectively [3].

There is little to no data on the crystallization kinetics of metallic glasses under pulsed laser irradiation, primarily because the low optical contrast between their crystalline and amorphous phases limits the ability to study the transformation with standard ultrafast optical techniques. However, with the high temporal and spatial resolution capabilities of the DTEM[4-6], rapid nucleation events resulting from pulsed laser irradiation can be directly observed, and nucleation rates can be quantified. This paper will compare the crystallization kinetics of amorphous NiTi films measured *in situ* in a conventional TEM, at slow heating rates, with those determined by high-time-resolution DTEM imaging during rapid pulsed heating.

Sputter-deposited amorphous NiTi films were studied by *in situ* TEM annealing experiments using a Gatan single-tilt heating stage in brightfield imaging mode in a JEOL 200CX. Figure 1 shows a series of TEM images taken at nine different times during isothermal crystallization occurring at 768 K. The 250 nm thick NiTi film fully crystallized within 60 s at this temperature, and displayed nucleation and growth rates similar to those reported by Lee et al[7]. The final microstructure is primarily coarse-

grained (grain size >2 μm), but also contained small nanocrystalline regions that formed at the later stages of crystallization (examples are indicated by white arrows in Figure 1).

The transformed volume fraction and average crystallite size were determined as a function of time using Digital Micrograph® grayscale-thresholding and particle analysis routines. Using the same kinetic analysis as Lee et al. [7], we fit the transformed volume fraction as a function of time with the Johnson-Mehl-Avrami-Kolmogrov equation[8,9],

$$X(t) = 1 - \exp[(-k(t-\tau))^n] \quad (1)$$

where the crystallized fraction, *X(t)*, increases exponentially with time (*t*) as a function of the kinetic parameter (*k*), the incubation time (τ), and the Avrami coefficient (*n*). The kinetic parameter is defined as follows,

$$k = k_o \exp(-Q/\kappa T) \quad (2)$$

where the prefactor, k_o, is typically taken as the phonon frequency (10^{13} s^{-1}), *Q* is the activation energy, κ is the Boltzman constant, and *T* is temperature. The Avrami parameter, *n*, is used to describe the type of nucleation and dimensionality of growth. For example, slow polymorphic crystallization processes in NiTi have an Avrami coefficient of 3, denoting homogeneous nucleation with 2-D growth. Fitting the data in Figure 1 (b) with Eqn. 1 and setting n=3, the kinetic parameter was determined to be 0.053 s^{-1}. Assuming that the maximum value of the pre-exponential factor does not exceed the Debye frequency (10^{13} s^{-1}), the maximum crystallization activation energy (*Q*) can be estimated from Eqn. 2 to be ~220 kJ mol^{-1} (2.3 eV). Typical activation energies for polymorphic crystallization of NiTi thin films measured by DSC[10-13] or *in situ* TEM[7,14-16] range from 250 to 500 kJ mol^{-1} (2.6 to 5.2 eV). The slightly lower upper bound to the

activation energy observed in the present experiments suggests the foil may be titanium rich[11].

The kinetic parameter (for an Avrami coefficient of 3) can also be estimated by using the steady state nucleation rate J_o and average crystallite growth velocity V_o for polymorphic crystallization:

$$k = \sqrt[3]{(\pi/3) J_o V_o^2} \tag{3}$$

The nucleation rate was determined by observing the number of newly formed grains as a function of time and normalizing it to the areal fraction of crystallized material, $[1/(1-X(t_i))]J(t_i) = dN/dt = (N_i - N_{i-1})/(t_i - t_{i-1})$, where the number of crystals per area, N_i, observed at a given time t_i associated with image frame i, was counted to determine the instantaneous rate, $J(t_i)$, that was then normalized to the areal fraction of untransformed material, 1-X(t_i). After 15 s, the nucleation rate at 768 K reached a steady state value of ~ 0.045 μm^{-2} s^{-1}, which is comparable to the rate observed by Lee et al. (0.017 nuclei per μm^{-2} s^{-1})[7].

The growth velocity was calculated by tracking the circumference and shape of the growing crystals. The linear regression fit of grain size as a function of time for several grains was used to determine the effective crystallization growth velocity. This analysis was repeated for several different crystals, yielding a growth velocity before impingement of 0.142± 0.005 μm s^{-1}.

Using the steady state values for growth velocity and nucleation rate, the kinetic parameter k was determined by Eqn. 3 to be ~0.097±0.012 s^{-1}. The value is nearly twice the value determined from the fit in Figure 1(b), however this is a relatively small difference, corresponding to a slightly lower activation energy of 205 kJ mol^{-1} (2.12eV).

Some of the discrepancy between the measurements may be due to changes in the nucleation rate which tended to decrease in the later stages of crystallization. In summary, our results from the slow heating experiments are roughly consistent with the reports in the literature.

In situ pulsed laser crystallization experiments were conducted in a DTEM that is capable of capturing irreversible, transient material dynamics with nanosecond time resolution [4,6,17]. The high time resolution is afforded by a pulsed UV laser driven photoemission source that replaces the conventional thermionic emitter in the microscope. To observe the crystallization process in NiTi, a sputtered thin film specimen is first irradiated with a 12 ns, 1064 nm 'pump' laser pulse to heat the sample (at rates exceeding 10^{10} K s^{-1}) and induce crystallization. Then, after a predefined time delay, a UV 'probe' laser is triggered and that irradiates a photocathode, generating a 15ns pulse of photoelectrons in the microscope column that has sufficient intensity to produce a snap-shot image of the crystallization process. Further details regarding this instrument are given in references[4,6,17]. In addition to this synchronized snap-shot, pulsed electron probe images are also acquired both before laser heating, and again several minutes after the synchronized probe pulse after the specimen has cooled to room temperature. More than 500 individual pump-probe experiments were carried out to collect data for this work.

Figure 2 shows an example of a series of nanosecond time-resolved images from two DTEM experiments taken at pump-probe time delays of 1.5 and 1.75μs. In both sets of images, the center of the pulsed laser spot (120 μm $1/e^2$ diameter) is located near the lower left-hand corner of the image. At an estimated laser induced temperature rise of

1200 K (at a laser fluence of 72 mJ cm^{-2}) determined by previously reported calibration methods[18], no discernable crystallites were observed before 500 ns, after which a high density of ~2-4 nuclei per μm^2 was found (see Figure 2 b). At 1.75 μs the higher temperature regions in the center of the laser irradiated area were fully crystallized, while the lower temperature surrounding regions began to nucleate crystallites. Overall, the pulsed laser crystallization exhibits a radially propagating crystallization front with varying nucleation rates and crystallization times related to the temperature gradient across the Gaussian laser heated zone. The threshold temperature for crystallization was estimated to be about 850K.

The nucleation rate was estimated by the same method used for the conventional *in situ* TEM heating experiments. However, instead of analyzing a sequence of video frames from a single heating experiment, the DTEM method requires multiple experiments in which images are acquired at different time delays between the pump and probe pulses. The number of crystallized grains per unit area having an average estimated temperature are then determined. Figure 3(a) shows the nucleation rate as a function time for a region of the foil at a temperature of 1200K. The nucleation rate is sluggish at the onset, indicating the existence of a significant incubation time, estimated to be 400-500ns. A steady state value of ~10^6 nuclei μm^{-2} s^{-1} is then reached before the rate diminishes during the later stages of crystallization. The error bars in Figure 3(a) express the large variation in the data. This scatter is partly due to the shot-to-shot variation in laser energy, and to variations in film thickness and surface topography, making it difficult to precisely estimate the laser-induced temperature.

The crystallized fraction as a function of probe-pulse time delay was also measured, and is shown in Figure 3(b). The data were fit using Eqn. 1 as was done in the analysis of the conventional TEM data in Figure 1(b). Assuming again that n=3 the kinetic parameter (k) and incubation time (τ) were determined to be 7.78 x 10^5 s^{-1} and 408 ns, respectively. Using Eqn. 2 and assuming k_0 to be 10^{13} s^{-1}, the approximate activation energy for crystallization was found to be 164 kJ mol^{-1} (1.7 eV), which is lower than the activation energy at 768K (2.3 eV) determined for isothermal crystallization. Finally, the growth velocity can be estimated by inserting the observed the steady state nucleation rate and kinetic parameter into Eqn. 3, yielding a value ~6.7x10^5 μm s^{-1}. For the 15 ns duration of the probe pulse used, this value corresponds to an image blur of 10 nm, consistent with the sharpness of the images in Figure 2.

The growth velocity can also be approximated from the grain size in the crystallized film using the expression, $\bar{d} = 1.2\sqrt[3]{V_o / J_o}$, where the average grain size ($\bar{d}$) is constrained by ratio between the growth (V_o) and nucleation rate (J_o) [3,16]. Using the measured nucleation rate and grain size of 0.95±0.05 μm, the growth velocity would be calculated as $V_o = \bar{d}^{\,3} J_o / 1.2^3$, giving V_o = 4.96x10^5, similar to the 6.7x10^5 value determined by eqn. 3.

The growth velocity is relatively slow compared to values predicted by the lower temperature data in both Wang et al.[14] and Lee et al.[16]. Their values of V_o were greater than 10^7 μm s^{-1} which would produce an image blur of a few microns. The lower growth velocities in the present work may be explained by composition of the sputtered thin film used in our study which is believed to have been slightly enriched in titanium with respect to equiatomic stoichiometry. This would require ejection of Ti ahead of the

crystallization front[19]. This mechanism has been observed in slow annealing experiments, but its influence on the kinetic parameters may not scale in the manner described by Eqns. 1 and 2.

In summary, the kinetic parameters measured under pulse laser irradiation at high temperatures differ significantly from those calculated from low temperature DSC and TEM experiments. Using the high time resolution imaging capabilities of the DTEM, these parameters were quantitatively measured in strongly driven conditions (high temperatures and ultra-fast heating) that cannot be accessed by standard techniques such as DSC. Having such kinetic data now allows to tailor the grain sizes of NiTi films with pulsed laser annealing and thus the shape memory properties and device operation. Moreover, the DTEM experimental technique can be extended to other technologically important solid state transformations, and to scientifically interesting systems such as α-Si, α-Ge or $Ge_xSb_yTe_z$, providing data on nucleation behavior inaccessible by other methods.

ACKNOWLEDGEMENTS

This work was performed under the auspices of the U.S. Department of Energy by Lawrence Livermore National Laboratory and Michigan State University, and was supported by the Office of Science, the Office of Basic Energy Sciences, the Division of Materials Sciences and Engineering, and the U.S. Department of Energy under contract No. DE-AC52-07NA27344.

REFERENCES

[1] P. Krulevitch, A. P. Lee, P. B. Ramsey, J. C. Trevino, J. Hamilton, and M. A. Northrup, Journal of Microelectromechanical Systems **5,** 270-282 (1996).

[2] Y. C. Her, C. W. Chen, and C. L. Wu, Journal of Applied Physics **99,** - (2006).

[3] X. Wang and J. J. Vlassak, Scripta Materialia **54,** 925-930 (2006).

[4] T. LaGrange, G. H. Campbell, B. Reed, M. Taheri, J. B. Pesavento, J. S. Kim, and N. D. Browning, Ultramicroscopy **108,** 1441-1449 (2008).

[5] J. S. Kim, T. LaGrange, B. W. Reed, M. L. Taheri, M. R. Armstrong, W. E. King, N. D. Browning, and G. H. Campbell, Science **321,** 1472-1475 (2008).

[6] T. LaGrange, M. R. Armstrong, K. Boyden, C. G. Brown, G. H. Campbell, J. D. Colvin, W. J. DeHope, A. M. Frank, D. J. Gibson, F. V. Hartemann, J. S. Kim, W. E. King, B. J. Pyke, B. W. Reed, M. D. Shirk, R. M. Shuttlesworth, B. C. Stuart, B. R. Torralva, and N. D. Browning, Applied Physics Letters **89,** - (2006).

[7] H. J. Lee, H. Ni, D. T. Wu, and A. G. Ramirez, Applied Physics Letters **87,** 114102 (2005).

[8] W. A. Johnson and R. F. Mehl, Transactions of the American Institute of Mining and Metallurgical Engineers **135,** 416-442 (1939).

[9] M. Avrami, Journal of Chemical Physics **7,** 1103-1112 (1939).

[10] M. J. Vestel, D. S. Grummon, R. Gronsky, and A. P. Pisano, Acta Materialia **51,** 5309-5318 (2003).

[11] J. M. Ting and P. Chen, Journal Of Vacuum Science & Technology A-Vacuum Surfaces And Films **19,** 2382-2387 (2001).

[12] K. T. Liu and J. G. Duh, Journal Of Non-Crystalline Solids **353,** 1060-1064 (2007).

[13] J. J. Kim, P. Moine, and D. A. Stevenson, Scripta Metallurgica **20,** 243-248 (1986).

[14] X. Wang, M. Rein, and J. J. Vlassak, Journal of Applied Physics **103,** - (2008).

[15] H. Ni, H. J. Lee, and A. G. Ramirez, Journal of Materials Research **20,** 1728-1734 (2005).

[16] H. J. Lee, H. Ni, D. T. Wu, and A. G. Ramirez, Applied Physics Letters **87,** 124102 (2005).

[17] W. E. King, G. H. Campbell, A. Frank, B. Reed, J. F. Schmerge, B. J. Siwick, B. C. Stuart, and P. M. Weber, Journal of Applied Physics **97,** - (2005).

[18] T. LaGrange, G. H. Campbell, P. E. A. Turchi, and W. E. King, Acta Materialia **55,** 5211-5224 (2007).

[19] M. J. Vestel and D. S. Grummon, Materials Science And Engineering A-Structural Materials Properties Microstructure And Processing **378,** 437-442 (2004).

FIGURE LEGENDS

Figure 1. a) Sequence of video frames taken from *in situ* TEM crystallization studies Time indicated in lower right-hand corner. Black arrow indicate the first observable crystallite. White arrow indicates the final region to undergo crystallization. b) The crystallization fraction as a function of time determined by image analysis of the video frames. The data was fit (solid line) using Johnson-Mehl-Avrami-Kolmogorov rate theory assuming an Avrami parameter of 3.

Figure 2. Series of 15ns exposure pulsed electron images, a) left image taken before laser heating, middle image taken 1.5μs after laser strikes the foil, right image taken after foil cools to room temperature, b) similar series of images from different region on the foil and with the middle image taken 1.75 μs after the pump laser irradiates the specimen. It should be noted that the solid white features are pin-holes in the as-fabricated thin films.

Figure 3. a) Measured nucleation and b) crystallization rate for pulse laser heating to a temperature of 1200K. Error bar on times are ~10ns.

FIGURES

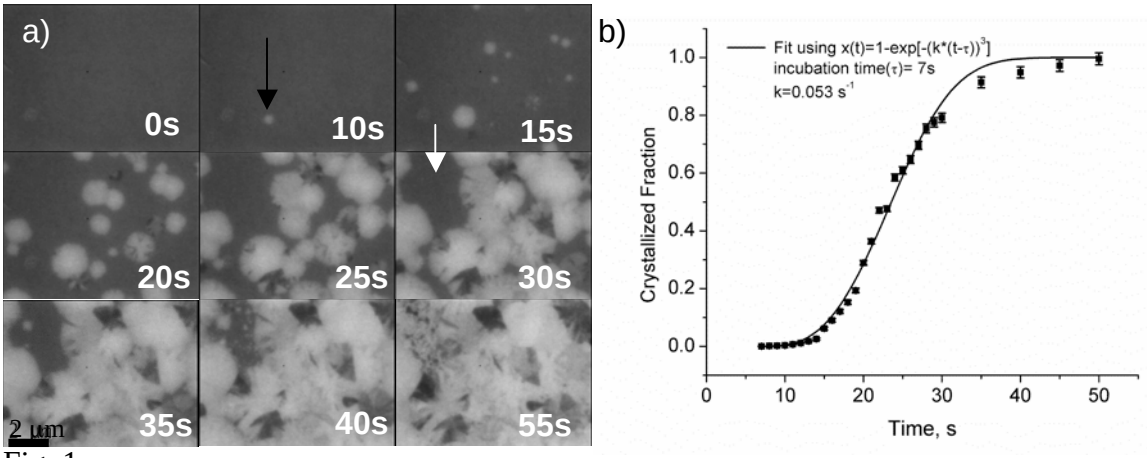

Fig. 1

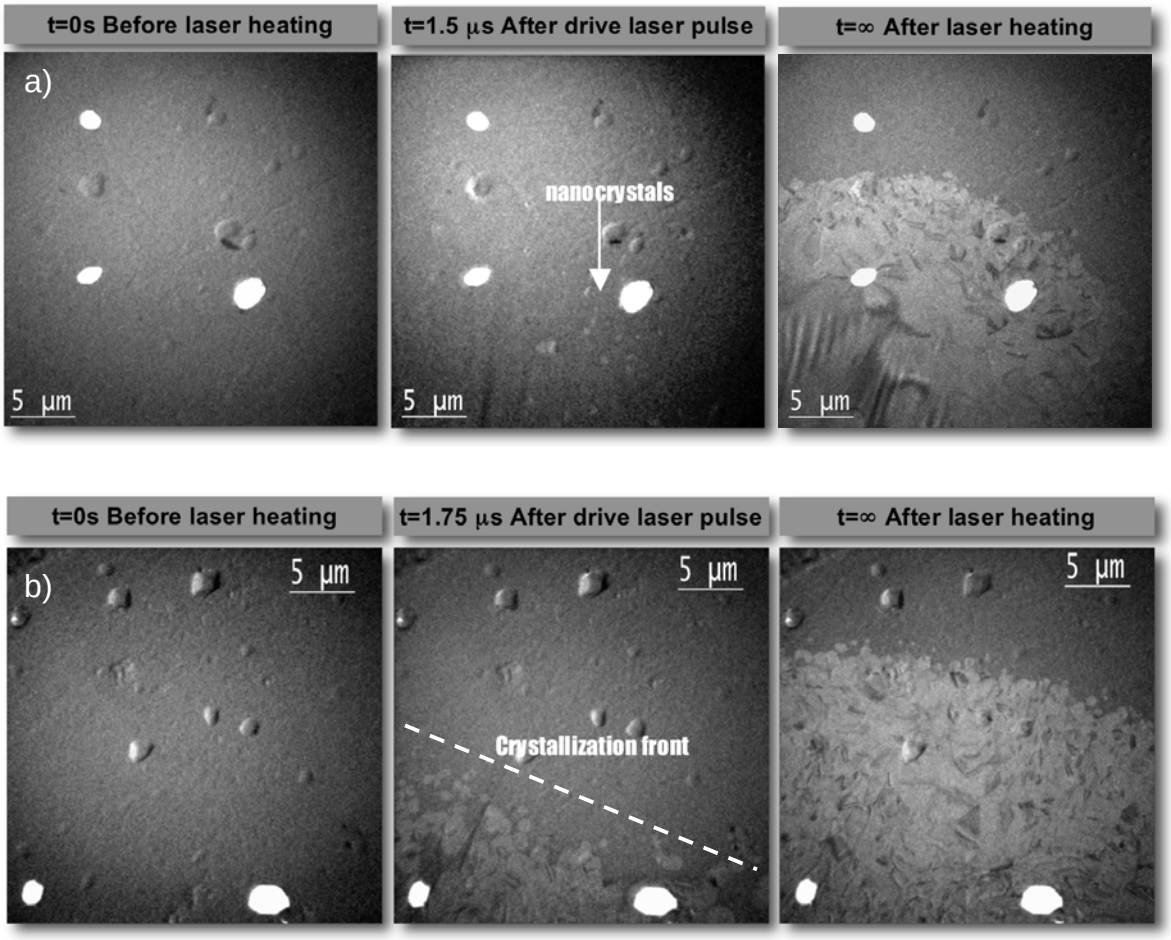

Fig. 2

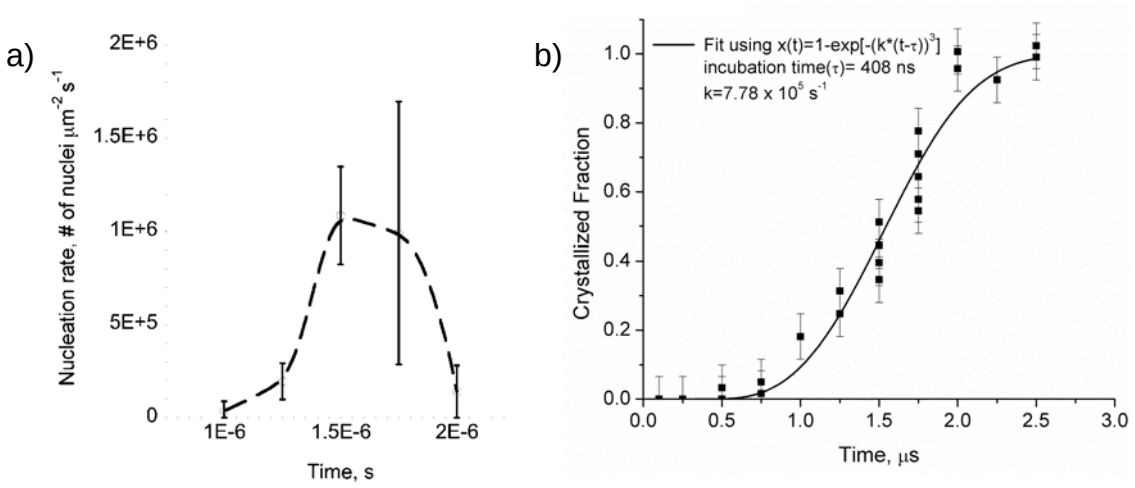
a)
Nucleation rate, # of nuclei μm^{-2} s^{-1}
2E+6
1.5E+6
1E+6
5E+5
0
1E-6
1.5E-6
2E-6
Time, s
b)
Fit using x(t)=1-exp[-(k*(t-τ))^3]
incubation time(τ)= 408 ns
k=7.78 x 10^5 s^{-1}
Crystallized Fraction
1.0
0.8
0.6
0.4
0.2
0.0
0.0
0.5
1.0
1.5
2.0
2.5
3.0
Time, μs